Hindawi
Mathematical Problems in Engineering
Volume 2022, Article ID 8208342, 11 pages
https://doi.org/10.1155/2022/8208342

Research Article

Energy Transport and Effectiveness of Thermo-Sloutal Time's Relaxation Theory in Carreau Fluid with Variable Mass Diffusivity

Muhammad Irfan,[1] **Muhammad Shoaib Anwar**,[2] **Humara Sardar**,[3] **Masood Khan**,[4] **and Waqar Azeem Khan**[5,6]

[1]*Department of Mathematical Sciences Federal Urdu University of Arts, Sciences & Technology, Islamabad 44000, Pakistan*
[2]*Department of Mathematics, University of Jhang, Jhang 35200, Pakistan*
[3]*Department of Mathematics, Rawalpindi Women University 6th Road, Satellite Town, Rawalpindi, Punjab 46300, Pakistan*
[4]*Department of Mathematics, Quaid-I-Azam University, Islamabad 44000, Pakistan*
[5]*Nonlinear Analysis and Applied Mathematics (NAAM) Research Group Department of Mathematics Faculty of Science King AbdulAziz University, Jeddah 21589, Saudi Arabia*
[6]*Department of Mathematics, Mohi-ud-Din Islamic University, Nerian Sharif, Islamabad, Azad Jammu & Kashmir 12010, Pakistan*

Correspondence should be addressed to Muhammad Irfan; muhammad.irfan@uow.edu.pk

Received 21 November 2021; Revised 27 February 2022; Accepted 8 March 2022; Published 18 April 2022

Academic Editor: Yong Aaron Tan

Two different frames' temperature creates thermal transport that gives advantage in energy fabrication in the power sector, burning in microscopic devices, and for remedy transport through heat transfer in materials. Here the article scrutinizes the transport of head utilizing the thermo-sloutal time's relaxation, and aspects of non-Fick's flux with variable conductivity and mass diffusivity in Carreau fluid have been elaborated. The magnetic aspect is also examined in a bidirectional stretched surface. The numerical procedure of ODEs via bvp4c method has been aimed at the solutions of influential parameters. The portrayal of influential factors is also presented. The intensifying behavior has been noted on concentration and temperature scattering when inconsistent thermal conductivity and variable mass diffusivity boost up. Furthermore, the temperature and concentration relaxation times are incorporated for the better understanding of the flow problem. The assessments of current article with former literature are also presented for the endorsement of outcomes.

1. Introduction

Throughout the past years, it has been noticed that many substances of industrial importance, particularly of multiphase behavior like polymeric melts, foams, emulsions, suspensions, dispersions, and slurries do not validate the Newtonian law of viscosity. In the literature, such fluids are named as, non-Newtonian liquids, nonlinear liquids, and rheological complex liquids. In non-Newtonian fluids [1–10], the apparent viscosity is not persistent and is a function of shear rate, and shear stress. In fact, under suitable conditions, the apparent viscosity of nonlinear materials is a function of kinematic history of fluid elements, flow geometry and shear rate. Non-Newtonian models come into play when major variations in the shear rate of fluid elements. Various rheological models had been considered to cater the behavior of non-Newtonian materials. In 1972, Carreau suggested the Carreau fluid model; for instance see Carreau [11] and Carreau et al. [12]. It remains with this physical model that the viscosity can be characterized for a boundless shear rates range. Carreau fluid viscosity is considered as a function of shear rate, infinite shear rate, relaxation time, power law index, and zero shear rates. Pantokratoras [13] elucidated a particular Carreau model with the help of controlling number "n." For, $0 < n < 1$, fluid behavior is considered as shear-thinning, shear-thickening for $n > 1$, and for $n = 1$, Newtonian. So, the Carreau fluid acts as the classical Newtonian fluid at smaller values of shear rate and power law fluid at larger values of shear rate. Recently, Salahuddin [14] considered the numerical solutions of Carreau fluid flow and the flow was generated by the stretching cylinder. Transport mechanism in MHD nano-Carreau fluid flow with microorganism's gyrotactic flow was discussed by Elayarani et al. [15].

In literature, analysis of transport mechanisms in the Carreau fluid flow mainly considered classical Fourier equations for heat and mass distributions. Classical Fourier equations are parabolic equations that lead to a paradox of heat and mass flux, i.e. an initial contribution of energy and concentration delivers an immediate experience by a whole system. The paradox was addressed by Cattaneo [16] with the addition of relaxation time. Christov [17] contributed to the theory of Cattaneo with the introduction of Oldroyd, an upper-convected derivative in place of an unsteady rate of change. So in this article, instead of classical Fourier equations we have adopted the Cattaneo–Christov transport mechanism for standard Carreau fluid flow. Reddy and Kumar [18] analyzed the stream line study of heat transfer in micro-polar fluid flow above a melting boundary. Ibrahim and Gadisa [19] discussed the simulations for transfer of heat in convective Oldroyd-B fluid flow using Finite Element Method (FEM). Flow was generated by a stretching sheet with heat absorption. Utilizing the theory of Cattaneo-Christov numerous researchers have analyzed these aspects in diverse models [20–24].

Here disclose the properties of thermo-sloutal time's relaxation in 3D magneto Carreau fluid considering variable mass diffusivity and variable conductivity. The existent Carreau fluid model is proficient in describing the phenomena of shear thinning and shear thickening. The blood flow via tapered arteries with stenosis is the noteworthy application of Carreau fluid. Moreover, blood flow via tapered arteries with stenosis has fascinated the consideration of numerous researchers. Because flows via arteries pose grave healthiness threats and are a foremost reason of humanity and sickness in the technologically advanced domain. Reduction of an artery, or stenosis, can outcome from considerable plaque pledge, and possibly will reason a severe decline in blood flow. The plaques possibly will also be disrupted off into elements, or emboli, which might be lodged in an artery downstream. In intellectual arteries the threat of embolism is that the cracked spots are passed into the brain, frustrating neurological indications or a stroke. The impacts of numerous factors are examined graphically. Additionally, assessment tables via limiting sense with (bvp4c) and analytically (HAM) are reported.

2. Development of Physical Model

2.1. Rheological Models. The reported Carreau fluid model has the following Cauchy stress tensor (τ^*):

$$\tau^* = -pI + \mu(\dot{\gamma})A_1, \tag{1}$$

with

$$\mu(\dot{\gamma}) = (\mu_0 - \mu_\infty)\left[1 + (\Gamma\dot{\gamma})^2\right]^{n-1/2} + \mu_\infty, \text{and } \dot{\gamma} = \sqrt{\frac{1}{2}tr\left(A_1^2\right)}. \tag{2}$$

Now considering $\mu_\infty \ll \mu_0$ and $\mu_\infty = 0$, we have

$$\tau^* = -pI + \mu_0\left[1 + (\Gamma\dot{\gamma})^2\right]^{n-1/2}A_1. \tag{3}$$

The stress components are reported to be

$$\begin{aligned}
\tau^*_{xx} &= \mu_0\left[1 + (\Gamma\dot{\gamma})^2\right]^{n-1/2}\left(2\frac{\partial u}{\partial x}\right),\\
\tau^*_{yy} &= \mu_0\left[1 + (\Gamma\dot{\gamma})^2\right]^{n-1/2}\left(2\frac{\partial v}{\partial y}\right),\\
\tau^*_{zz} &= \mu_0\left[1 + (\Gamma\dot{\gamma})^2\right]^{n-1/2}\left(2\frac{\partial w}{\partial z}\right),\\
\tau^*_{xy} &= \tau^*_{yx} = \mu_0\left[1 + (\Gamma\dot{\gamma})^2\right]^{n-1/2}\left(\frac{\partial v}{\partial x} + \frac{\partial u}{\partial y}\right),\\
\tau^*_{xz} &= \tau^*_{zx} = \mu_0\left[1 + (\Gamma\dot{\gamma})^2\right]^{n-1/2}\left(\frac{\partial w}{\partial x} + \frac{\partial u}{\partial z}\right),\\
\tau^*_{yz} &= \tau^*_{zy} = \mu_0\left[1 + (\Gamma\dot{\gamma})^2\right]^{n-1/2}\left(\frac{\partial w}{\partial y} + \frac{\partial v}{\partial z}\right).
\end{aligned} \tag{4}$$

2.2. Problem Description. Here examine the characteristics of inconsistent thermal conductivity and variable diffusivity of mass in Carreau fluid flow to bidirectional stretched surface. Velocities of the fluid in x–and y–directions are reflected to be $u = ax$ and along the vertical direction $v = by$; where $a, b > 0$ and occurrence of flow exists in area $z > 0$ see Figure 1. The non-Fick's mass, and non-Fourier's heat fluxes scheme considering magnetic influence have been studied. These norm yields the following Carreau fluid equations [2, 3, 5]:

$$\frac{\partial u}{\partial x} + \frac{\partial v}{\partial y} + \frac{\partial w}{\partial z} = 0,$$

$$u\frac{\partial u}{\partial x} + v\frac{\partial u}{\partial y} + w\frac{\partial u}{\partial z} + \frac{\sigma B_0^2 u}{\rho_f} - \nu\frac{\partial^2 u}{\partial z^2}\left[1 + \Gamma^2\left(\frac{\partial u}{\partial z}\right)^2\right]^{\frac{n-1}{2}} + \nu\Gamma^2(n-1)\left[1 + \Gamma^2\left(\frac{\partial u}{\partial z}\right)^2\right]^{\frac{n-3}{2}}\left(\frac{\partial u}{\partial z}\right)^2\left(\frac{\partial^2 u}{\partial z^2}\right) = 0,$$

$$u\frac{\partial v}{\partial x}+v\frac{\partial v}{\partial y}+w\frac{\partial v}{\partial z}+\frac{\sigma B_0^2 v}{\rho_f}-\nu\frac{\partial^2 v}{\partial z^2}\left[1+\Gamma^2\left(\frac{\partial v}{\partial z}\right)^2\right]^{\frac{n-1}{2}}+\nu\Gamma^2(n-1)\left[1+\Gamma^2\left(\frac{\partial v}{\partial z}\right)^2\right]^{\frac{n-3}{2}}\left(\frac{\partial v}{\partial z}\right)^2\left(\frac{\partial^2 v}{\partial z^2}\right)=0,$$

$$u\frac{\partial T}{\partial x}+v\frac{\partial T}{\partial y}+w\frac{\partial T}{\partial z}-\frac{1}{(\rho c)_f}\frac{\partial}{\partial z}\left(K(T)\frac{\partial T}{\partial z}\right)+\Gamma_T\left[\begin{array}{c}u^2\frac{\partial^2 T}{\partial x^2}+2uv\frac{\partial^2 T}{\partial x\,\partial y}+u\frac{\partial u}{\partial x}\frac{\partial T}{\partial x}+u\frac{\partial v}{\partial x}\frac{\partial T}{\partial y}+u\frac{\partial w}{\partial x}\frac{\partial T}{\partial z}\\ +v^2\frac{\partial^2 T}{\partial y^2}+2vw\frac{\partial^2 T}{\partial y\,\partial z}+v\frac{\partial u}{\partial y}\frac{\partial T}{\partial x}+v\frac{\partial v}{\partial y}\frac{\partial T}{\partial y}+v\frac{\partial w}{\partial y}\frac{\partial T}{\partial z}\\ +w^2\frac{\partial^2 T}{\partial z^2}+2uw\frac{\partial^2 T}{\partial x\,\partial z}+w\frac{\partial u}{\partial z}\frac{\partial T}{\partial x}+w\frac{\partial v}{\partial z}\frac{\partial T}{\partial y}+w\frac{\partial w}{\partial z}\frac{\partial T}{\partial z}\end{array}\right]=0,$$

$$u\frac{\partial C}{\partial x}+v\frac{\partial C}{\partial y}+w\frac{\partial C}{\partial z}-\frac{\partial}{\partial z}\left(D(C)\frac{\partial C}{\partial z}\right)+\Gamma_C\left[\begin{array}{c}u^2\frac{\partial^2 C}{\partial x^2}+2uv\frac{\partial^2 C}{\partial x\,\partial y}+u\frac{\partial u}{\partial x}\frac{\partial C}{\partial x}+u\frac{\partial v}{\partial x}\frac{\partial C}{\partial y}+u\frac{\partial w}{\partial x}\frac{\partial C}{\partial z}\\ +v^2\frac{\partial^2 C}{\partial y^2}+2vw\frac{\partial^2 C}{\partial y\,\partial z}+v\frac{\partial u}{\partial y}\frac{\partial C}{\partial x}+v\frac{\partial v}{\partial y}\frac{\partial C}{\partial y}+v\frac{\partial w}{\partial y}\frac{\partial C}{\partial z}\\ +w^2\frac{\partial^2 C}{\partial z^2}+2uw\frac{\partial^2 C}{\partial x\,\partial z}+w\frac{\partial u}{\partial z}\frac{\partial C}{\partial x}+w\frac{\partial v}{\partial z}\frac{\partial C}{\partial y}+w\frac{\partial w}{\partial z}\frac{\partial C}{\partial z}\end{array}\right]=0,$$

$$U_w(x)=u=ax, V_w(y)=v=by, w=0, T=T_w, C=C_w \text{ at } z=0,$$

$$u\longrightarrow 0, v\longrightarrow 0, w\longrightarrow 0, T\longrightarrow T_\infty, C\longrightarrow C_\infty, \text{as} z\longrightarrow\infty. \tag{5}$$

The variable aspect of thermal conductivity $K(T)$ and mass diffusivity $D(C)$, respectively, elaborated as

$$K(T)=k_1\left(1+\varepsilon_1\frac{T-T_\infty}{\Delta T}\right),\quad D(C)=k_2\left(1+\varepsilon_2\frac{C-C_\infty}{\Delta C}\right). \tag{6}$$

2.3. Appropriate Transformations. Letting

$$u=axf'(\eta),\quad v=ayg'(\eta),\quad w=-\sqrt{a\nu}[f(\eta)+g(\eta)],\quad \theta(\eta)=\frac{T-T_\infty}{T_w-T_\infty},\quad \phi(\eta)=\frac{C-C_\infty}{C_w-C_\infty},\quad \eta=z\sqrt{\frac{a}{\nu}}. \tag{7}$$

(6) and (7) yield the following expressions:

$$f'''\left[1+We_1^2 f''^2\right]^{n-3/2}\left[1+nWe_1^2 f''^2\right]-f'^2+f''(f+g)+M^2 f'=0. \tag{8}$$

$$g'''\left[1+We_2^2 g''^2\right]^{n-3/2}\left[1+nWe_2^2 g''^2\right]-g'^2+g''(f+g)+M^2 g'=0. \tag{9}$$

$$(1+\varepsilon_1\theta)\theta''+\varepsilon_1\theta'^2+\Pr(f+g)\theta'-\Pr\delta_T\left[(f+g)(f'+g')\theta'+(f+g)^2\theta''\right]=0. \tag{10}$$

$$(1+\varepsilon_2\phi)\phi''+\varepsilon_2\phi'^2+Sc(f+g)\phi'-Sc\delta_C\left[(f+g)(f'+g')\phi'+(f+g)^2\phi''\right]=0. \tag{11}$$

$$f(0)=0,\quad g(0)=0,\quad f'(0)=1,\quad g'(0)=\alpha,\quad \theta(0)=1,\quad \phi(0)=1. \tag{12}$$

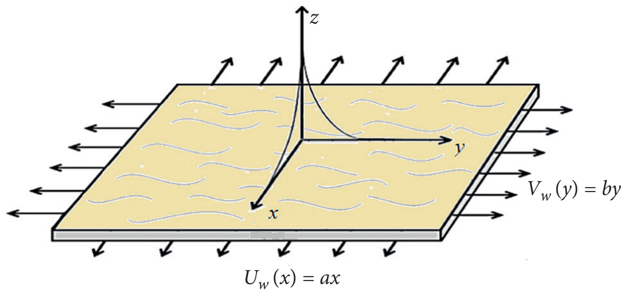

FIGURE 1: Flow configuration and coordinate system.

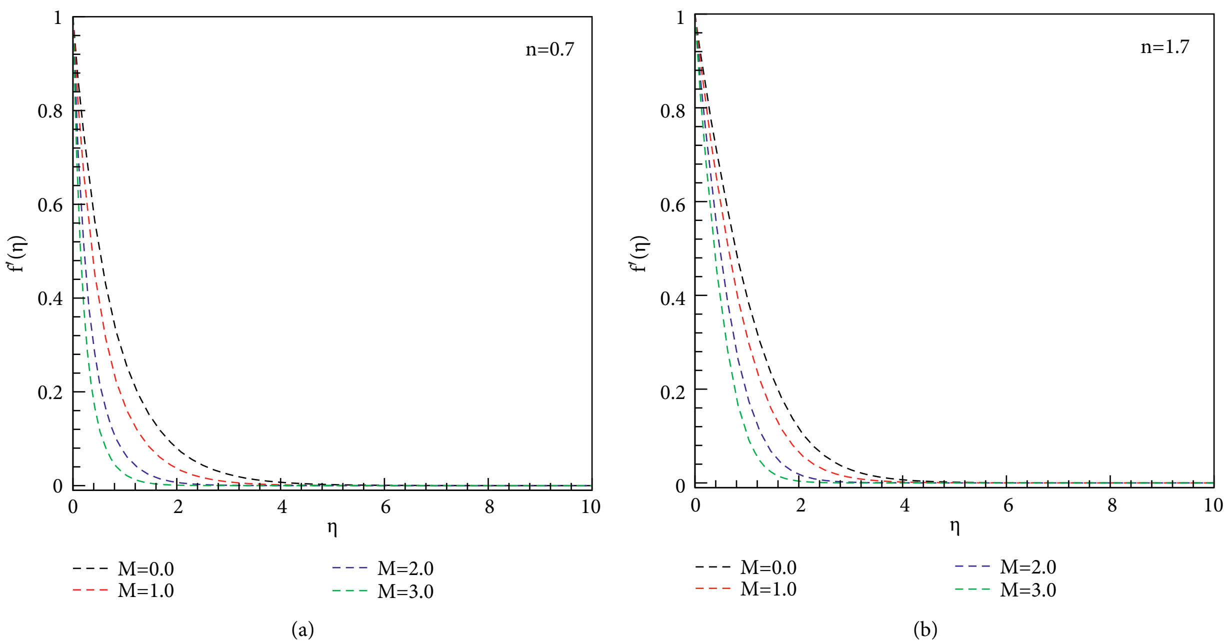

FIGURE 2: (a, b) Plot of η vs. $f'(\eta)$ for M.

$$f' \longrightarrow 0, \quad g' \longrightarrow 0, \quad \theta \longrightarrow 0, \quad \phi \longrightarrow 0, \quad as \quad \eta \longrightarrow \infty. \tag{13}$$

Here, $(We_1, We_2) = (\sqrt{\Gamma^2 a U_w^2/\nu}, \sqrt{\Gamma^2 a v_w^2/\nu})$ signify the local Weissenberg numbers, $M(= \sigma B_0^2/\rho_f a)$ magnetic field, $(\delta_T, \delta_C) = (a\Gamma_T, a\Gamma_C)$ thermal and concentration relaxation time factors, $\alpha(= b/a)$ ratio of stretching rates factor, and $Sc(= \nu/D)$ the Schmidt number and.

3. Physical Amounts

3.1. The Coefficients of Skin Friction C_{fx} and C_{fy}. The quantities of this interest are

$$C_{fx} = \frac{\tau_{xz}}{1/2\rho U_w^2} \quad \text{and} \quad C_{fy} = \frac{\tau_{yz}}{1/2\rho U_w^2}. \tag{14}$$

Dimensionless form of the above equation:

$$\frac{1}{2} C_{fx} \mathrm{Re}_x^{1/2} = f''(0)\left[1 + We_1^2 f''^2(0)\right]^{n-1/2},$$
$$\frac{1}{2}\left(\frac{U_w}{V_w}\right) C_{fy} \mathrm{Re}_x^{1/2} = g''(0)\left[1 + We_2^2 g''^2(0)\right]^{n-1/2}. \tag{15}$$

Here, $Re_x = ax^2/\nu$ stands for Reynolds number.

4. Numerical Approach (bvp4c)

The numerical procedure of ODEs via bvp4c method has been disclosed here by discretize procedure and we revise the equations (8)–(13) into first-order differential systems:

$$
\begin{aligned}
& f = p_1, f' = p_2, f'' = p_3, f''' = p_3', g = p_4, g' = p_5, g'' = p_6, g''' = p_6', \theta = p_7, \theta' = p_8, \theta'' = p_8', \phi = p_9, \phi\prime = y_{10}, \phi'' = p_{10}', \\
& p_3' = \frac{-(p_1 + p_4)p_3 + p_2^2 - M^2 p_2}{\Omega_1}; \quad \Omega_1 = \left(1 + nWe_1^2 p_3^2\right) * \left(1 + We_1^2 p_3^2\right)^{\frac{n-3}{2}}, \\
& p_6' = \frac{-(p_1 + p_4)p_6 + p_5^2 - M^2 p_5}{\Omega_2}; \quad \Omega_2 = \left(1 + nWe_2^2 p_6^2\right) * \left(1 + We_2^2 p_6^2\right)^{\frac{n-3}{2}} \\
& p_8' = \frac{-\Pr(p_1 + p_4)p_8 - \varepsilon_1 p_8^2 + \Pr\delta_T\left[(p_1 + p_4)(p_2 + p_5)p_8\right]}{\Omega_3}; \Omega_3 = (1 + \varepsilon_1 p_7) - \Pr\delta_T (p_1 + p_4)^2, \\
& p_{10}' = \frac{-Sc(p_1 + p_4)p_{10} + Sc\delta_C\left[(p_1 + p_4)(p_2 + p_5)p_{10}\right]}{\Omega_4}; \Omega_4 = (1 + \varepsilon_2 p_9) - Sc\delta_C (p_1 + p_4)^2, \\
& p_1(0) = 0, p_2(0) = 1, p_2(\infty) = 0; p_4(0) = 0, p_5(0) = \alpha, p_5(\infty) = 0; p_7(0) = 1, p_7(\infty) = 0; p_9(0) = 1, p_9(\infty) = 0.
\end{aligned}
\tag{16}
$$

5. Analysis of Results

Here, variable aspects of mass diffusivity and thermal conductivity considering non-Fick's mass, and non-Fourier's heat and fluxes have been studied with magnetic properties. Here $\Gamma_T = \Gamma_C = 0.1, \varepsilon_1 = \varepsilon_2 = 0.4$, $M = \alpha = 0.5$, $\Pr = Sc = 1.5, We_1 = We_2 = 2.5$ have been stated fixed values excepting particular in graphs for $n = 0.7$ and $n = 1.7$.

5.1. Velocity $f\prime(\eta)$ for M. Figures 2(a) and 2(b) determine the performance of magnetic factor M on velocity component $f\prime(\eta)$. The higher M falloff the velocity component for both cases $(n = 0.7)$ and $(n = 1.7)$. Physically, higher magnetic field creates a body force named as Lorentz force, which faces the fluid gesture and, therefore, it diminishes the fluid independence of movement. Consequently, when magnetic flux growths, the retardation force rises and this struggle existing to the flow is accountable for diminishing the liquid velocity.

5.2. Temperature $\theta(\eta)$ for M, ε_1, Pr, and Γ_T. Figures 3(a), 3(b), 4(a), and 4(b) envision the plots of magnetic factor M and variable conductivity factor ε_1 on Carreau fluid temperature scattering. Here noted that $\theta(\eta)$ intensifies when M and ε_1 enhances. When M increases, the Carreau fluid temperature rises and similar performance is acknowledged for ε_1. When M intensify the Lorentz force improves which form additional struggle to the liquid motion to convert the energy into heat. This information reasons to the intensifying of $\theta(\eta)$. Significantly, $\theta(\eta)$ growths for augmenting values of ε_1 as a consequence of enormous heat transport amount from the sheet to the solid and as a result the $\theta(\eta)$ boosts up.

Figures 5(a), 5(b), 6(a), and 6(b) explore temperature of the Carreau fluid with the values of the Prandtl number Pr and the thermo relaxation factor Γ_T which falloff $\theta(\eta)$. The Carreau fluid temperature decays for larger Pr. As thermal diffusivity and Pr have differing relationship, this fact decays $\theta(\eta)$. When $\Pr \gg 1$, the momentum diffusivity controls the performance; however, $\Pr \ll 1$, the thermal diffusivity controls. Furthermore, Γ_T decline $\theta(\eta)$. Physically, the fluid material needs an extra interval for heat transportation to its neighboring fundamentals which improves the gradient of temperature. Hence, $\theta(\eta)$ decay for Γ_T.

5.3. Concentration $\phi(\eta)$ for Γ_C, ε_2, and Sc. The portrayals of Figures 7(a) and 7(b) along with Figures 8(a) and 8(b) scrutinize performance of mass relaxation factor Γ_C and mass diffusivity ε_2 concentration field. The field of concentration, $\phi(\eta)$ decays for Γ_C; but, enhances for ε_2. Here conflicting enactments have been noted for Γ_C and ε_2 for both values of $(n = 0.7)$ and $(n = 1.7)$. When Γ_C raised the concentration field falls. Physically, the mass relaxation time factor is high and liquid elements need much time to diffuse when Γ_C enhancing which display declining behavior of $\phi(\eta)$. The advanced mass diffusivity factor increases the mass diffusivity which causes the higher mass transportation. Therefore $\phi(\eta)$ intensifies. The performance of Schmith number Sc for the values of $(n = 0.7)$ and $(n = 1.7)$ has been examined in Figures 9(a) and 9(b) on concentration. The solute of Carreau fluid decays for intensifying Sc. Physically, Sc is the relation between mass and momentum diffusivities. When Sc upturned, the mass diffusivity falls off. Therefore, the concentration field declines.

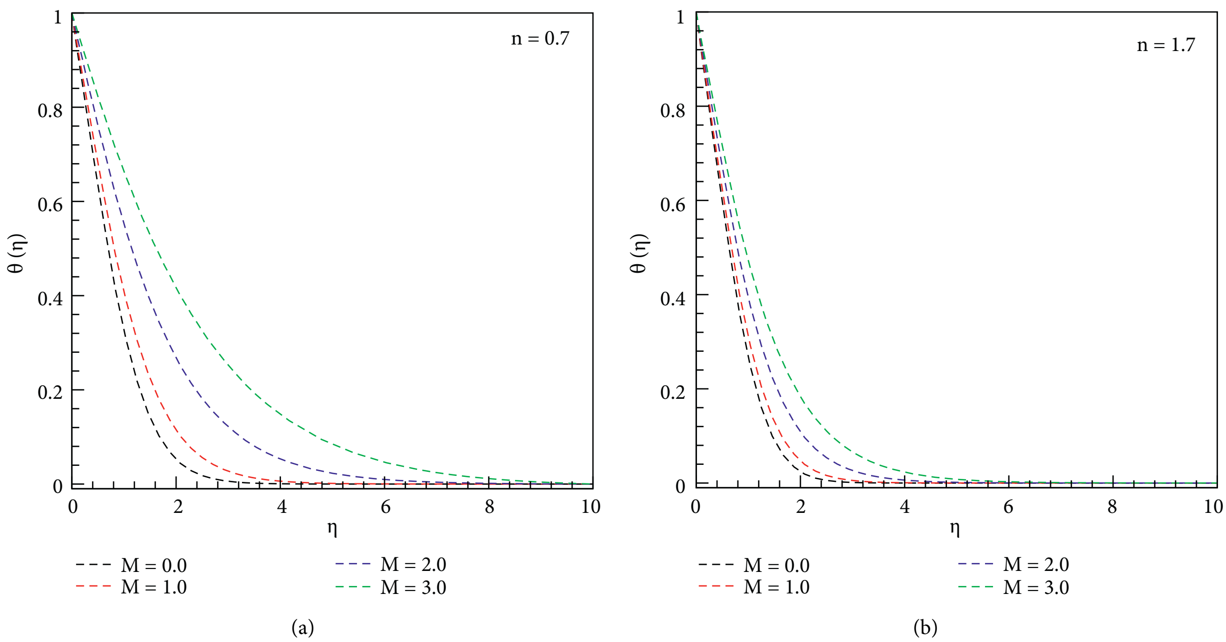

Figure 3: (a, b) Plot of η vs. $\theta(\eta)$ for M.

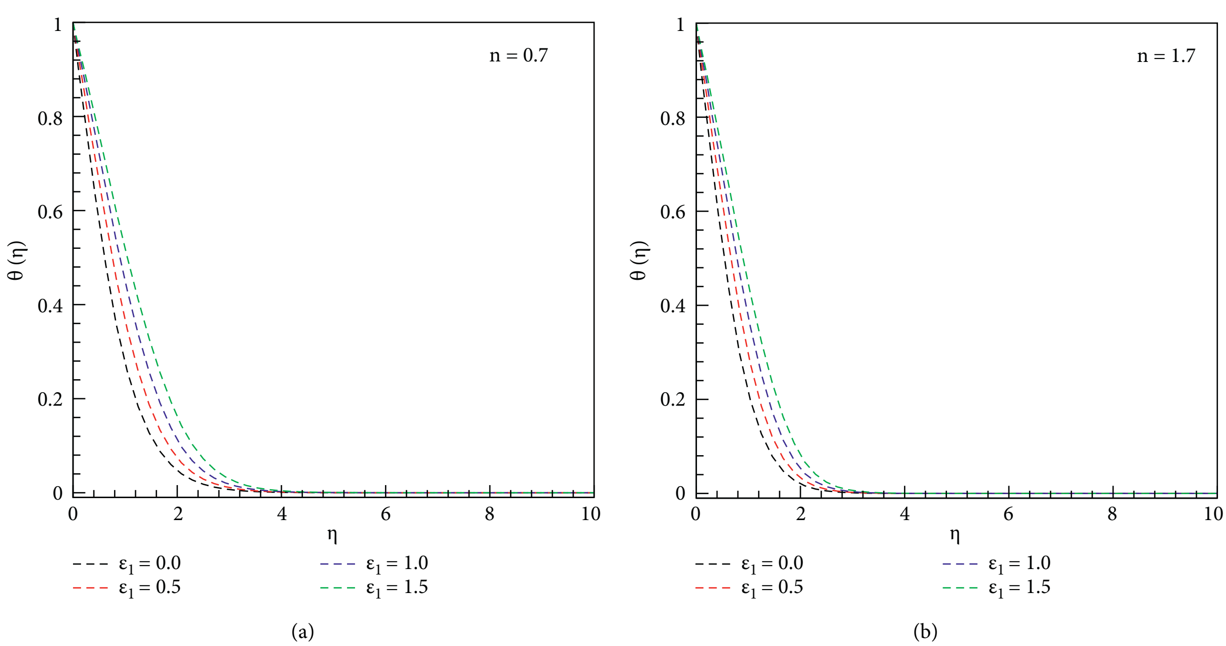

Figure 4: (a, b) Plot of η vs. $\theta(\eta)$ for ε_1.

5.4. Table of Skin Friction Coefficients. Table 1 structured for larger values of M an d α for $1/2C_{fx}Re_x^{1/2}$ and $1/2\,(U_w/V_w)C_{fy}Re_x^{1/2}$ for both instances $n = 0.7$ and $n = 1.7$. Here noted that the magnitude of $1/2C_{fx}Re_x^{1/2}$ and $1/2\,(U_w/V_w)C_{fy}Re_x^{1/2}$ increases when M an d α intensifies.

5.5. Comparison of bvp4c and HAM. Additionally, the HAM and bvp4c graphical comparisons for Newtonian case are reported in Figure 10 for $f\prime(\eta)$ an d $g\prime(\eta)$. Here, excellent portrayal are noted between both the methodologies.

To elaborate the comparison of $-\theta'(0)$ in limiting circumstances for diverse values of ε_1, Pr, and α, respectively, Tables 2 and 3 are acknowledged. These tables indicate a brilliant outcome associated with former literatures.

6. Closing Remarks

Here the essentials of thermo-sloutal time's relaxation in magnetite Carreau liquid with inconsistent aspects of mass diffusivity and thermal conductivity have been examined. The upcoming direction and significance of this model is

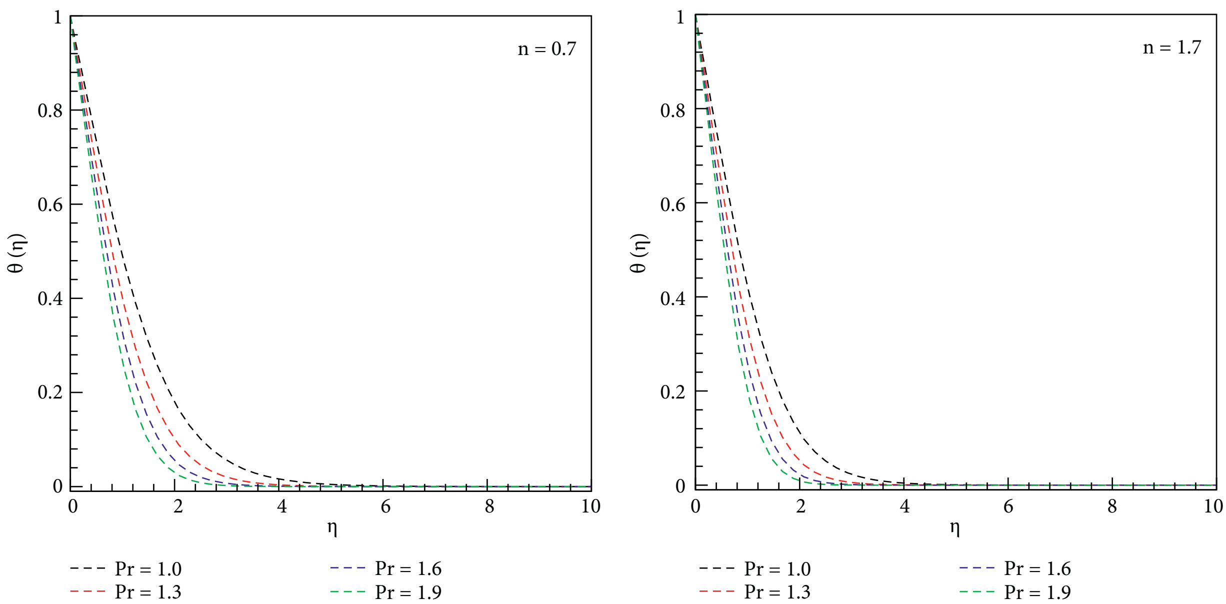

(a) (b)

Figure 5: (a, b) Plot of η vs. $\theta(\eta)$ for Pr.

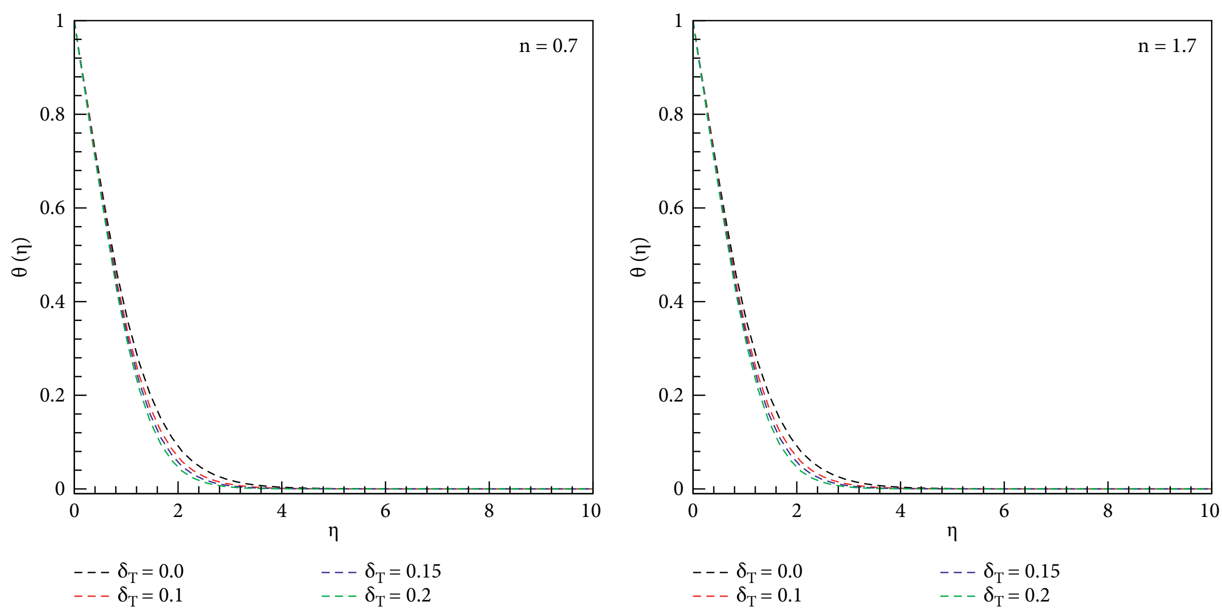

(a) (b)

Figure 6: (a, b) Plot of η vs. $\theta(\eta)$ for δ_T.

that blood flow via tapered arteries with a stenosis is the essential use of Carreau fluid model because this model deals with the phenomena of shear thinning/thickening fluids. Furthermore, this model is extended for calculating the multiple solutions and also for curved surfaces. The salient particulars of this analysis are acknowledged as

(i) The magnetic factor M declined the velocity field.

(ii) The Carreau fluid temperature exaggerated for ε_1, however falloffs for δ_T.

(iii) The larger M the temperature field is improved for $n = 0.7\, an\, d\, n = 1.7$.

(iv) Opposite influences were noted for $\Gamma_C\, an\, d\, \varepsilon_2$ on concentration scattering.

(v) Outstanding outcomes have been examined in limiting cases for $-\theta'(0)$.

(vi) The exceptional graphical depictions are plotted for comparisons of HAM and bvp4c of Carreau fluid model.

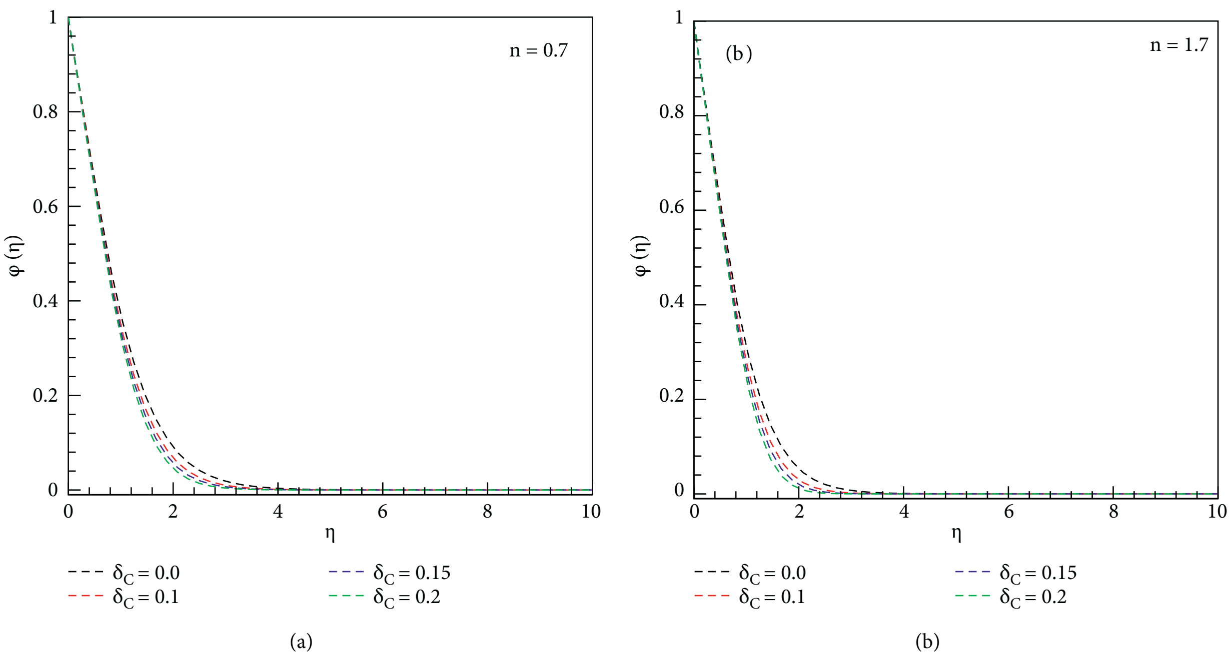

Figure 7: (a, b) Plot of η vs. $\phi(\eta)$ for δ_C.

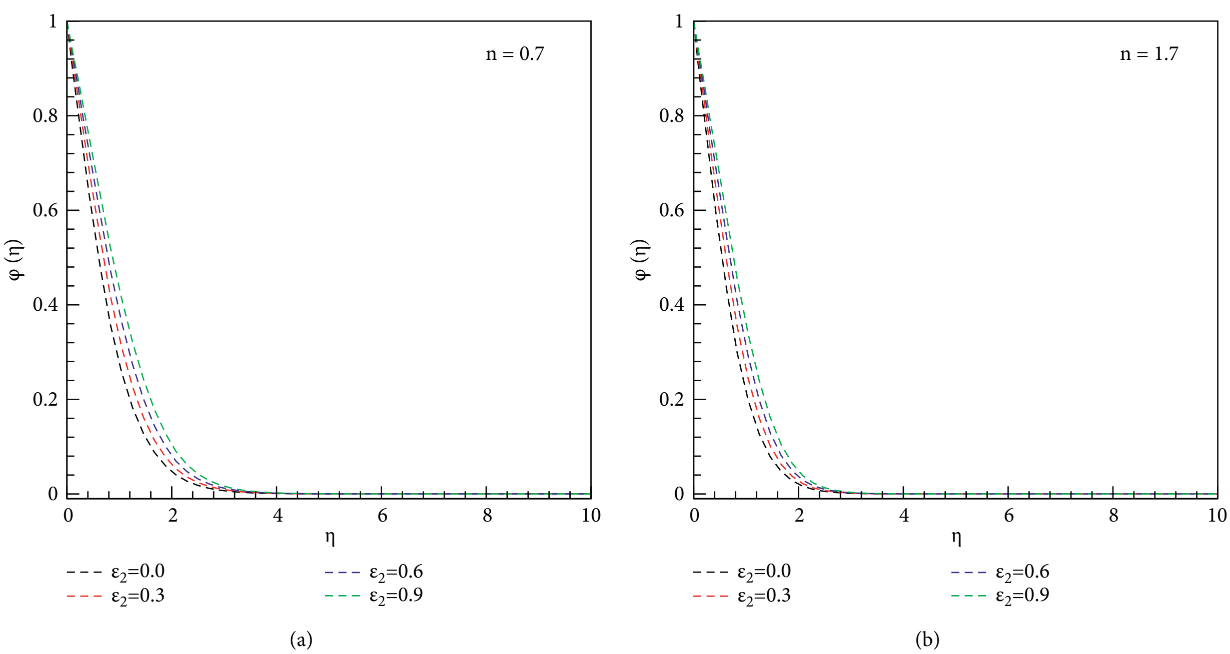

Figure 8: (a, b) Plot of η vs. $\phi(\eta)$ for ε_2.

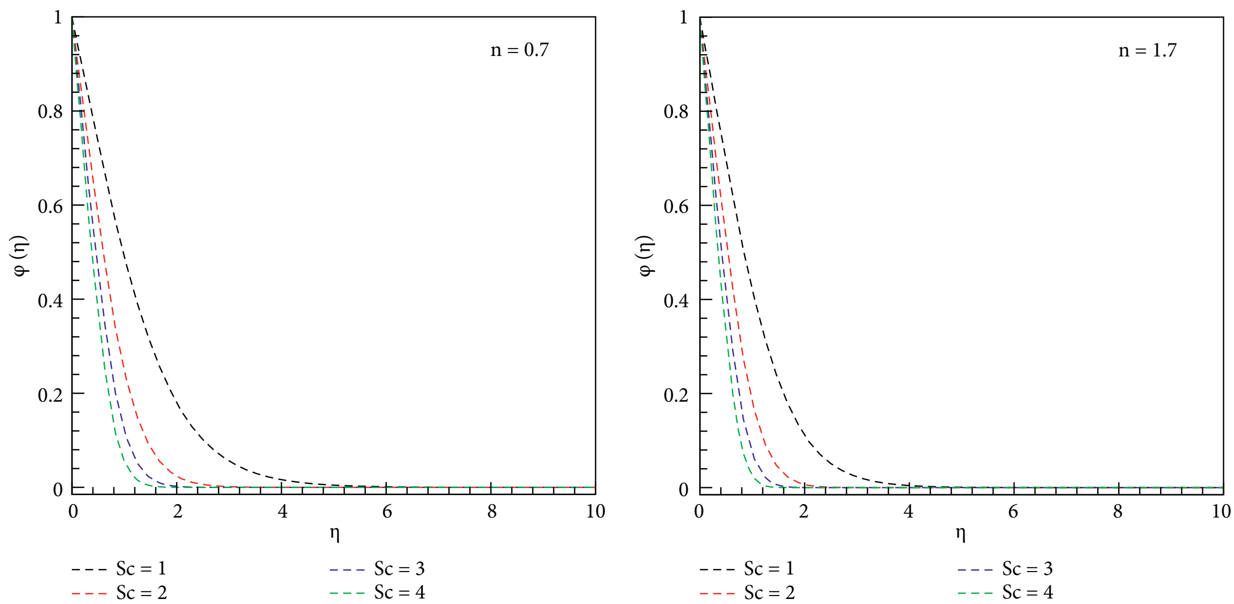

(a) (b)

Figure 9: (a, b) Plot of η vs. $\phi(\eta)$ for Sc.

Table 1: Outcomes of skin friction coefficients when $We_1 = We_2 = 2.5$.

M	α	$1/2C_{fx}Re_x^{1/2}$		$1/2\,(U_w/V_w)C_{fy}Re_x^{1/2}$	
		$n = 0.7$	$n = 1.7$	$n = 0.7$	$n = 1.7$
0.5	0.5	−2.75267	−6.28875	−0.735299	−1.17469
1.0		−3.91194	−9.92461	−1.097060	−1.88793
1.5		−5.72221	−16.5755	−1.666760	−3.15998
0.5	0.7	−2.85709	−6.69579	−1.41209	−2.70100
	0.8	−2.90692	−6.90700	−1.86225	−3.87658
	0.9	−2.95537	−7.12294	−2.39147	−5.40309

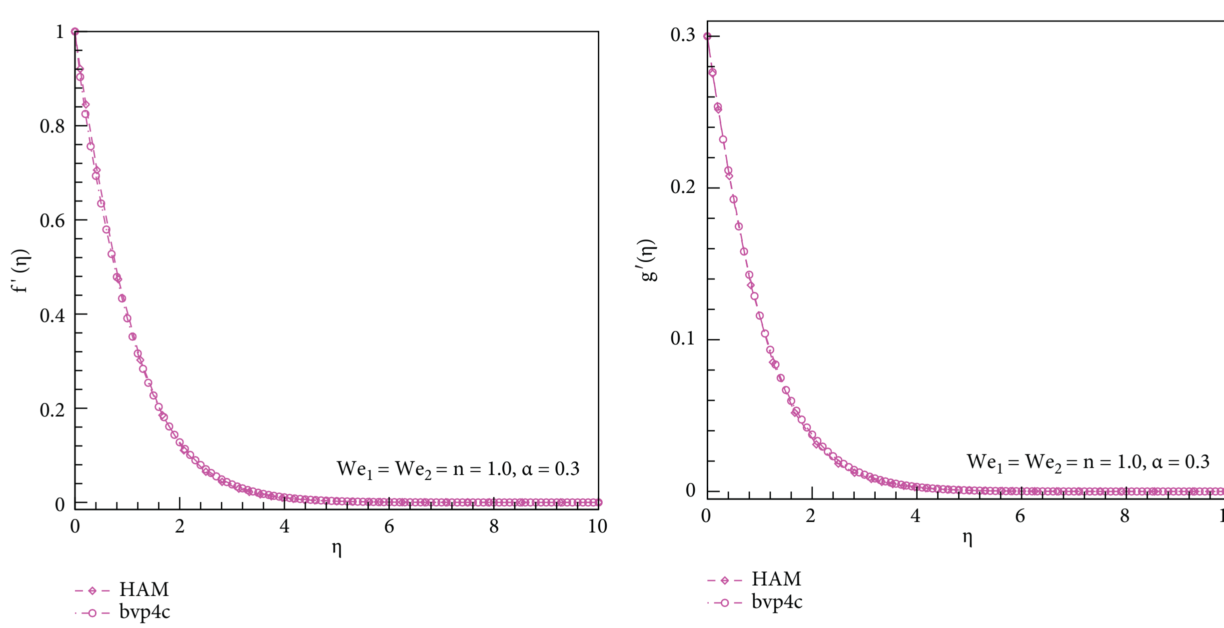

(a) (b)

Figure 10: (a, b) Plot of η vs. $f'(\eta)$ *an d* $g\prime(\eta)$ for HAM and bvp4c comparison.

Table 2: Outcomes of $-\theta'(0)$ for ε_1 and Pr when $We_1 = We_2 = \Gamma_T = \Gamma_C = \alpha = \varepsilon_2 = Sc = 0$ and $n = 1$ are fixed.

ε_1	Pr	$-\theta'(0)$	
		Ref. [25]	Present (bvp4c)
0.2	1.3	0.604568	0.60457302
0.3		0.569570	0.56957494
0.4		0.539040	0.53904539
0.2	1.5	0.664040	0.66404537
	1.7	0.719773	0.71978160
	2.0	0.797638	0.79765199

Table 3: Outcomes of $-\theta'(0)$ for α when $We_1 = We_2 = \Gamma_T = \Gamma_C = \varepsilon_1 = \varepsilon_2 = Sc = 0$ and $n = 1$ are fixed.

α	$-\theta'(0)$		
	Ref. [26]	Ref. [27]	Present (bvp4c)
0.25	0.665933	0.665939	0.6659332
0.50	0.735334	0.735336	0.7353329
0.75	0.796472	0.796472	0.7964718

Abbreviations

Γ: Material constant
n: Power law index
μ_0: Zero and infinity shear rate viscosities
p: Pressure
μ_∞: Infinity shear rate viscosities
$\dot{\gamma}$: Shear rate
(u, v, w): Velocity components $[ms^{-1}]$
(x, y, z): Space coordinates $[ms^{-1}]$
$(\rho c)_f$: Heat capacity of fluid $[JK^{-1}.m^{-3}]$
ν: Kinematic viscosity $[m^2 s^{-1}]$
T: Temperature of fluid $[K]$
C: Concentration of fluid $[K]$
$K(T)$: Variable thermal conductivity
$D(C)$: Variable mass diffusivity
k_1: Thermal conductivity of $(W/m.K)$ surrounding
k_2: Mass diffusivity of surrounding
T_∞: Ambient fluid temperature $[K]$
C_∞: Ambient fluid concentration $[K]$
T_w: Wall temperature $[K]$
C_w: Wall concentration $[K]$
δ_T: Thermal relaxation time
δ_C: Solutal relaxation time
C_{fx}, C_{fy}: Skin friction coefficients
τ_{xz}, τ_{yz}: Surface shear stresses
We_1, We_2: Local Weissenberg numbers
α: Ratio of stretching rates parameter
Γ_T, Γ_C: Thermal and concentration relaxation time factors
M: Magnetic factor
Pr: Prandtl number
ε_1: Thermal conductivity factor
Sc: Schmidt number
ε_2: Mass diffusivity factor
HAM: Homotopy analysis method
ODEs: Ordinary differential equations
tr: Trace of a tensor
PDEs: Partial differential equations
α: Ratio of stretching rates parameter.

Data Availability

This is the theoretical analysis, and no data are used in this study.

Conflicts of Interest

The authors declare that they have no conflicts of interest.

References

[1] J. Sui, L. Zheng, and X. Zhang, "Boundary layer heat and mass transfer with Cattaneo-Christov double-diffusion in upper-convected Maxwell nanofluid past a stretching sheet with slip velocity," *International Journal of Thermal Sciences*, vol. 104, pp. 461–468, 2016.
[2] L. Liu, L. Zheng, F. Liu, and X. Zhang, "Anomalous convection diffusion and wave coupling transport of cells on comb frame with fractional Cattaneo-Christov flux," *Communications in Nonlinear Science and Numerical Simulation*, vol. 38, pp. 45–58, 2016.
[3] M. Khan, M. Irfan, W. A. Khan, and A. S. Alshomrani, "A new modeling for 3D Carreau fluid flow considering nonlinear thermal radiation," *Results in Physics*, vol. 7, pp. 2692–2704, 2017.
[4] A. S. Dogonchi and D. D. Ganji, "Impact of Cattaneo-Christov heat flux on MHD nanofluid flow and heat transfer between parallel plates considering thermal radiation effect," *Journal of the Taiwan Institute of Chemical Engineers*, vol. 80, pp. 52–63, 2017.
[5] M. Irfan, M. Khan, and W. A. Khan, "On model for three-dimensional Carreau fluid flow with Cattaneo-Christov double diffusion and variable conductivity: A numerical approach," *Journal of the Brazilian Society of Mechanical Sciences and Engineering*, vol. 40, no. 12, 2018.
[6] N. Acharya, S. Maity, and P. K. Kundu, "Differential transformed approach of unsteady chemically reactive nanofluid flow over a bidirectional stretched surface in presence of magnetic field," *Heat Transfer*, vol. 49, no. 6, pp. 3917–3942, 2020.
[7] N. Acharya, R. Bag, and P. K. Kundu, "Unsteady bio-convective squeezing flow with higher-order chemical reaction and second-order slip effects," *Heat Transfer*, vol. 50, no. 6, pp. 5538–5562, 2021.
[8] M. Waqas, "Diffusion of stratification based chemically reactive Jeffrey liquid featuring mixed convection," *Surfaces and Interfaces*, vol. 23, Article ID 100783, 2021.
[9] N. Acharya, "Spectral quasi linearization simulation on the radiative nanofluid spraying over a permeable inclined spinning disk considering the existence of heat source/sink," *Applied Mathematics and Computation*, vol. 411, Article ID 126547, 2021.
[10] N. Acharya, H. Mondal, and P. K. Kundu, "Spectral approach to study the entropy generation of radiative mixed convective couple stress fluid flow over a permeable stretching cylinder," *Proceedings of the Institution of Mechanical Engineers - Part C: Journal of Mechanical Engineering Science*, vol. 235, no. 15, pp. 2692–2704, 2021.
[11] P. J. Carreau, "Rheological equations from molecular network theories," *Transactions of the Society of Rheology*, vol. 16, Article ID 99127, 1972.

[12] P. J. Carreau, D. D. Kee, and M. Daroux, "An analysis of the viscous behaviour of polymeric solutions," *Canadian Journal of Chemical Engineering*, vol. 57, no. 2, pp. 135–140, 1979.

[13] A. Pantokratoras, "Non-similar blasius and sakiadis flow of a non-Newtonian carreau fluid," *Journal of the Taiwan Institute of Chemical Engineers*, vol. 56, pp. 1–5, 2015.

[14] T. Salahuddin, "Carreau fluid model towards a stretching cylinder: Using Keller box and shooting method," *Ain Shams Engineering Journal*, vol. 11, no. 2, pp. 495–500, 2020.

[15] M. Elayarani, M. Shanmugapriya, and P. Senthil Kumar, "Intensification of heat and mass transfer process in MHD carreau nanofluid flow containing gyrotactic microorganisms," *Chemical Engineering and Processing - Process Intensification*, vol. 160, Article ID 108299, 2021.

[16] C. Cattaneo, "Sulla conduzione del calore," *Atti Semin Mat Fis Univ Modena Reggio Emilia*, vol. 3, pp. 83–101, 1948.

[17] C. I. Christov, "On frame indifferent formulation of the Maxwell-Cattaneo model of finite-speed heat conduction," *Mechanics Research Communications*, vol. 36, no. 4, pp. 481–486, 2009.

[18] M. G. Reddy and K. G. Kumar, "Cattaneo-Christov heat flux feature on carbon nanotubes filled with micropolar liquid over a melting surface: A stream line study," *International Communications in Heat and Mass Transfer*, vol. 122, Article ID 105142, 2021.

[19] W. Ibrahim and G. Gadisa, "Finite element solution of nonlinear convective flow of Oldroyd-B fluid with Cattaneo-Christov heat flux model over nonlinear stretching sheet with heat generation or absorption," *Propulsion and Power Research*, vol. 9, no. 3, pp. 304–315, 2020.

[20] N. Acharya, K. Das, and P. K. Kundu, "Cattaneo-Christov intensity of magnetised upper-convected Maxwell nanofluid flow over an inclined stretching sheet: A generalised Fourier and Fick's perspective," *International Journal of Mechanical Sciences*, vol. 130, pp. 167–173, 2017.

[21] D. Lu, M. Mohammad, M. Ramzan, M. Bilal, F. Howari, and M. Suleman, "MHD boundary layer flow of Carreau fluid over a convectively heated bidirectional sheet with non-Fourier heat flux and variable thermal conductivity," *Symmetry*, vol. 11, no. 5, p. 618, 2019.

[22] S. Sarojamma, R. V. Lakshmi, P. V. S. Narayana, and I. L. Animasaun, "Exploration of the significance of autocatalytic chemical reaction and Cattaneo-Christov heat flux on the dynamics of a micropolar fluid," *J. Appl. Comput. Mechanics*, vol. 6, pp. 77–89, 2020.

[23] Y. J. Lim, M. N. Zakaria, S. Mohamad Isa, N. A. Mohd Zin, A. Q. Mohamad, and S. Shafie, "VON Kármán Casson fluid flow with Navier's slip and cattaneo-christov heat flux," *Case Studies in Thermal Engineering*, vol. 28, Article ID 101666, 2021.

[24] P. S. Reddy and P. Sreedevi, "Effect of Cattaneo - christov heat flux on heat and mass transfer characteristics of Maxwell hybrid nanofluid flow over stretching/shrinking sheet," *Physica Scripta*, vol. 96, no. 12, Article ID 125237, 2021.

[25] W. A. Khan, M. Irfan, and M. Khan, "An improved heat conduction and mass diffusion models for rotating flow of an Oldroyd-B fluid," *Results in Physics*, vol. 7, pp. 3583–3589, 2017.

[26] I.-C. Liu and H. I. Andersson, "Heat transfer over a bidirectional stretching sheet with variable thermal conditions," *International Journal of Heat and Mass Transfer*, vol. 51, no. 15-16, pp. 4018–4024, 2008.

[27] A. Munir, A. Shahzad, and M. Khan, "Convective flow of Sisko fluid over a bidirectional stretching surface," *PLoS One*, vol. 10, no. 6, Article ID e0130342, 2015.